Numerical Simulation of Freestream Waves Receptivity and Breakdown in Mach 6 Flow over Cone

Jia Lei[1] and Xiaolin Zhong[2]
Mechanical and Aerospace Engineering Department, UCLA, Los Angeles, CA, 90095

This paper presented direct numerical simulations of hypersonic boundary layer transition over cones in Mach 6 flow with zero angle of attack induced by fresstream waves. A disturbance pulse model that embraces a wide range of frequencies is introduced in the freestream to capture the receptivity response at different frequencies. Approach that breaks the direct numerical simulation into three parts: meanflow computation, linear receptivity simulation and nonlinear breakdown simulation is utilized. One test case has been completed using the three-step approach. The simulation is carried up to the early stage of breakdown. The preliminary result shows strong evidence of fundamental resonance mechanism during the early stage into breakdown.

Nomenclature

a	=	non-dimensional wave speed
e	=	total energy per unit volume
Fi	=	inviscid flux vector
Fv	=	viscous flux vector
F	=	frequency
M	=	Mach number
Pr	=	Prandtl number
P	=	pressure
R_n	=	nose radius
Re	=	Reynolds number
Re_n	=	Reynolds number based on the nose radius
s	=	distance along the cone surface from the nose tip
T	=	temperature
u, v, w	=	velocity components
ξ, η, ς	=	local curve-linear coordinates
y_n	=	local normal distance from cone surface
α	=	streamwise wave number
ω	=	angular frequency
μ	=	viscosity
ρ	=	density
τ	=	shear stress
Superscript *	=	dimensional quantity
Subscript ∞	=	freestream quantity

I. Introduction

The prediction of laminar-turbulent transition of hypersonic boundary layers is critically important to the development of hypersonic vehicles that are to be used for rapid global access[1]. Boundary layer transition has first-order impacts on aerodynamic heating, as well as drag and control of hypersonic vehicles. Extreme heat

[1] Graduate Student Researcher, MAE Department, UCLA, and AIAA Student Member. jxlei@ucla.edu
[2] Professor, MAE Department, UCLA, and AIAA Associate Fellow. xiaolin@seas.ucla.edu

transfer rates are arguably the prime constraint in the design of hypersonic aircraft. Some success has been obtained in predicting heating rates in laminar or fully turbulent flow, but accurate predictions in a transitional regime remain elusive. Uncertainty in heat transfer rate requires large factors of safety to be used in current vehicle designs. Improved computational accuracy could lead to significant improvements in hypersonic vehicle performance by allowing the removal of unnecessary weight in the thermal protection system. The success of transition and related heating prediction relies on the good understanding of the relevant physical mechanisms leading to transition. In spite of considerable efforts in experimental, theoretical, and numerical studies, many critical physical mechanisms underlying hypersonic boundary-layer transition are still poorly understood. Engineering design of hypersonic vehicles has mainly been based on transition criteria obtained by empirical correlations of experimental data. The e^n method, which predicts boundary layer transition based on normal-mode linear stability theory, is by far the most successful mechanism-based prediction method for transition prediction. Nevertheless, the e^n method suffers from a major drawback that it does not consider the effects of receptivity of the boundary layer to freestream wave disturbances. In reality, the transition location is very sensitive to the level of forcing disturbances[2].

Since 1990s, significant progress has been made by several research groups in DNS studies of fundamental mechanisms leading to nonlinear breakdown and transition of supersonic and hypersonic boundary layers [3-5]. In DNS studies, the full 3-D nonlinear Navier-Stokes equations are computed to simulate the development and nonlinear interaction of the disturbances waves. A number of transition mechanisms have been identified and studied. In some cases, transition was simulated up to the beginning of turbulence. Detailed information on the formation and evolution of transitional flow structures, as well as average heating rates and skin friction, could be obtained by the simulation. It was found that the transition mechanisms for supersonic boundary layers include secondary instability of either sub-harmonic or fundamental resonances [6]. By using DNS, Thumm [7] and Fasel et al. [8] discovered a new breakdown mechanism for a boundary layer at Mach 1.6, which they termed oblique breakdown. This breakdown to turbulence is initiated by the nonlinear wave interaction of two oblique instability waves with equal but opposite wave angles. The mechanisms have also been confirmed by many researchers, including Chang and Malik [9]. For supersonic flows, it was shown that oblique breakdown leads to a more rapid transition than the secondary instability mechanisms. It also requires much lower threshold disturbance amplitudes for the nonlinear development [10]. For these reasons, oblique breakdown has been suggested to be of practical importance for supersonic transition in low-disturbance environments [11, 12].

Husmeier and Fasel [13] did DNS studies of secondary instability mechanisms of hypersonic boundary layers over cones with a circular cross section. The computational domain is a cut-out section of the whole flow field (Fig.1). Though hypersonic boundary layer is most unstable to second-mode two-dimensional waves, their investigations indicated that secondary instability mechanisms involving two-dimensional waves appear to be of lesser importance in the nonlinear stages of breakdown. Instead, second-mode oblique waves at small wave angles, which are almost as amplified as second-mode two-dimensional waves, were found to dominate the nonlinear behavior. It seems that further studies are necessary in order to confirm this conclusions because extensive experimental results have pointed to the dominant of 2-D second mode before transition in hypersonic boundary layers [14, 15].

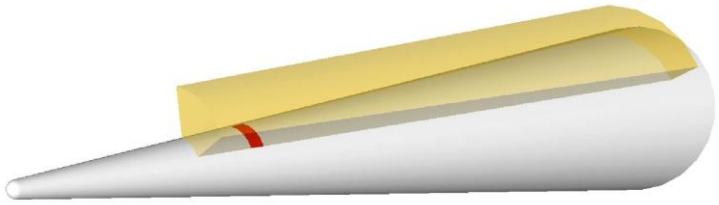

Fig.1. Computational domain used in Husmeier and Fasel's DNS simulation [13].

For hypersonic boundary layer transition, Pruett and his colleges did spatial DNS of hypersonic boundary layers of Mach 8 flow over a cone of eight-degree half angle [3, 4, 16]. The transitional state was triggered by a symmetric pair of oblique second-mode disturbances whose nonlinear interactions generate strong streamwise vorticity, which leads severe spanwise variations in the flow and eventual laminar breakdown. In their simulations, the PSE method was used to compute the weakly and moderately nonlinear initial stages of the transition process

and, thereby, to derive a harmonically rich inflow condition for the DNS. The strongly nonlinear and laminar-breakdown stages of transition were subsequently computed by well-resolved DNS.

Due to the enormous requirement on computer times and on computer memory, DNS studies on boundary layer transition have been limited to idealized cases of boundary layer response to imposed forcing waves. So far, the complete process of laminar-turbulent transition from leading edge to the beginning of transition has not been computed by direct numerical simulation. Such a task has been commonly regarded as beyond the capability, in terms of computational power of currently available computers. On the other hand, if possible, such simulation can have significant impact on the state of the art in transition prediction because the effects of freestream noise on transition location can be simulated by DNS. Therefore, it is necessary to develop, and validate a reliable DNS computational tool for the numerical simulation of the complete process of hypersonic boundary layer transition. Such simulation tool can be valuable in the prediction of surface heat transfer rates in transitional hypersonic boundary layers. In this paper, a three-step approach that separates the entire simulation into: meanflow calculation, linear receptivity simulation, and non-linear breakdown simulation, will be utilized to make the computational cost manageable. Also, this approach allows us to conduct multiple breakdown simulations with different inflow profiles without the need to repeat the receptivity simulation. Our ultimate goal is to use DNS to compute the complete transition process under realistic freestream noise and disturbances by dividing it into a three step process.

The objective of the paper is to setup the framework to perform a direct numerical simulation with natural disturbance spectrum coming from the freestream using a proposed three-step approach. The simulation will be carried out to reach the non-linear breakdown stage in transition. It is expected that the success of this DNS will help in understanding the flow physics and instability mechanisms during the non-linear breakdown process. Also, it will provide a reliable tool in predicting the transition in hypersonic boundary layer. In this paper, the DNS study is carried out on two different cone models over the Mach 6 flow. The flow condition is the same as the Mach 6 quiet tunnel at TAMU.

II. Numerical Method and Solution Strategy

A. Governing Equations

The governing equations are the unsteady compressible 3D Navier-Stokes equations, which can be written in the following conservative form:

$$\frac{\partial U^*}{\partial t^*} + \frac{\partial F_j^*}{\partial x_j^*} + \frac{\partial F_{vj}^*}{\partial x_j^*} = 0 \tag{1}$$

where $U^* = (\rho^*, \rho^* u_1^*, \rho^* u_2^*, \rho^* u_3^*, e^*)$, and superscript "*" represents dimensional variables. The F^* s are invicid and viscous flux terms that can be expanded as

$$F^*_j = \begin{Bmatrix} \rho u_j \\ \rho u_{j1} u_j + p\delta_{1j} \\ \rho u_{j2} u_j + p\delta_{1j} \\ \rho u_{j3} u_j + p\delta_{1j} \\ (e+p)u_j \end{Bmatrix} \quad \text{and} \quad F^*_{vj} = \begin{Bmatrix} 0 \\ \tau_{1j} \\ \tau_{2j} \\ \tau_{3j} \\ \tau_{jk} u_k - q_j \end{Bmatrix} \tag{2}$$

The Cartesian coordinates are denoted by (x_1^*, x_2^*, x_3^*) in tensor notation. In the current simulation of axisymmetric flow over blunt cones, x^* is the coordinate along the centerline of the cone pointing toward the downstream direction. The origin of coordinate is co-located with the center of spherical nose.

B. Numerical Scheme

A High-order shock-fitting code originally developed by Zhong [17] is used to compute the flow field bounded by the bow shock and cone surface. The flow variables behind the shock are determined by Rakine-Hugoniot relations across the shock and the characteristic compatibility equations. Since the performance of the linear stability analysis is very sensitive to the base flow solution, the base flow must be very accurate in order to obtain the reliable results on the linear stability analysis. The shock-fitting scheme had been tested and proven accurate and reliable by different test case.

C. Solution Strategy

We propose to tackle this problem by using our innovative approach of separating the linear receptivity simulation from the nonlinear breakdown simulation. In this way, we are able to make the computational cost manageable by breaking the whole simulation process into 3 major steps:

- **Step I: Mean Flow Simulation**. The high accuracy mean flow solution without any freestream disturbance is obtained using our high-order shock-fitting scheme. This is done with multiple zone procedure by cutting the whole computational zone along the cone surface into shorter subzones and marching the solution downstream as long as we needed.

- **Step II**: **Linear Receptivity Simulation.** In this step, a series of linear receptivity simulations are carried out with different types of freestream disturbances: fast acoustic wave, slow acoustic wave and entropy wave. They are imposed in the receptivity simulation to the mean flow solution in the freestream. In the receptivity simulation of each type of disturbance, multiple frequencies are imposed to better represent the freestream wave spectrum. The receptivity simulation will be carried all the way to the end of the linear growth region. This location can be estimated by LST analysis or by investigation of simulation result. The linear receptivity simulation is computationally much less expensive than the full scale 3D non-linear simulation due to the fact that the simulation is axis-symmetric in nature. So, a 2D simulation with significant less number of grid points is sufficient.

- **Step III**: **Non-linear Breakdown Simulation**. After finishing the receptivity simulation, the entrance condition for the 3D non-linear simulation can be constructed based on the solutions obtained from the linear simulation. The inflow boundary condition is obtained from the preceding linear receptivity simulations. Fourier decomposition is applied to separate disturbance waves into different frequencies. Therefore the inflow disturbance can be from freestream fast/slow acoustic wave, entropy waves and combination of all. In this paper, we only focus on using the disturbance profile from freestream fast acoustic waves for code testing purpose. A more realistic disturbance profile can be constructed to be consistent with those from experiments. Since the Fourier decomposition in time can be applied to separate the solution in linear region for different frequencies, we can rescale the magnitude of solution for each specified frequency to match the freestream noise spectrum in a typical experiment. Therefore, the complete transition process due to different freestream noise profile can be simulated by using the receptivity results. So that, we just need to do the receptivity simulation once for different cases of different freestream spectra and different noise amplitudes. We can simply rescale the magnitude of each frequency to match the freestream value in the spectrum. As a result, for various freestream disturbance profiles, only step three is repeated to investigate the effects of freestream noise levels on the location of boundary layer transition.

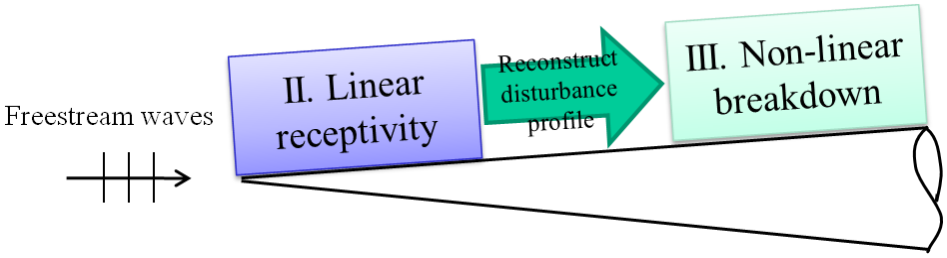

Fig. 2. Schematic of proposed simulation procedures to non-linear breakdown

III. Computation Setup

A. Flow Conditions

In the effort to collaborate with Hypersonic Transition Research Center, we continue our numerical study using the flow conditions that the experimental team at TAMU uses on their Mach 6 quiet tunnel. The detail flow conditions are listed below.

- $M_\infty = 5.91$
- $P_\infty^* = 622.84\,Pa$, $T_\infty^* = 56.35K$
- Wall temperature: $T_w =$ adibatic wall
- $\gamma = 1.4$, $\Pr = 0.72$, $R^* = 286.94 Nm/kgK$
- Freestream unit Reynolds number: $\mathrm{Re}_\infty^* = 9.25\times10^6\, m^{-1}$
- Blunt cone half angle: $\theta = 5^\circ$, the freestream flow has a zero angle of attack
- Parameters in Sutherland's viscosity law: $T_r^* = 288K$, $T_s^* = 110.33K$,
  $\mu_r^* = 0.17894\times10^{-4}\, kg/ms$

Using the cone geometry similar to TAMU quiet tunnel experiment team, we computed the mean flow solutions for two different cone models with different nose sharpness. First cone we computed is the similar to NASA Langley 93-10 model except that the nose radius is 0.125 inch. The second cone computed is a straight cone with 0.1 mm nose bluntness. In this paper, we will carry out the non-linear breakdown simulation using the cone model with nose radius of 0.1 mm only.

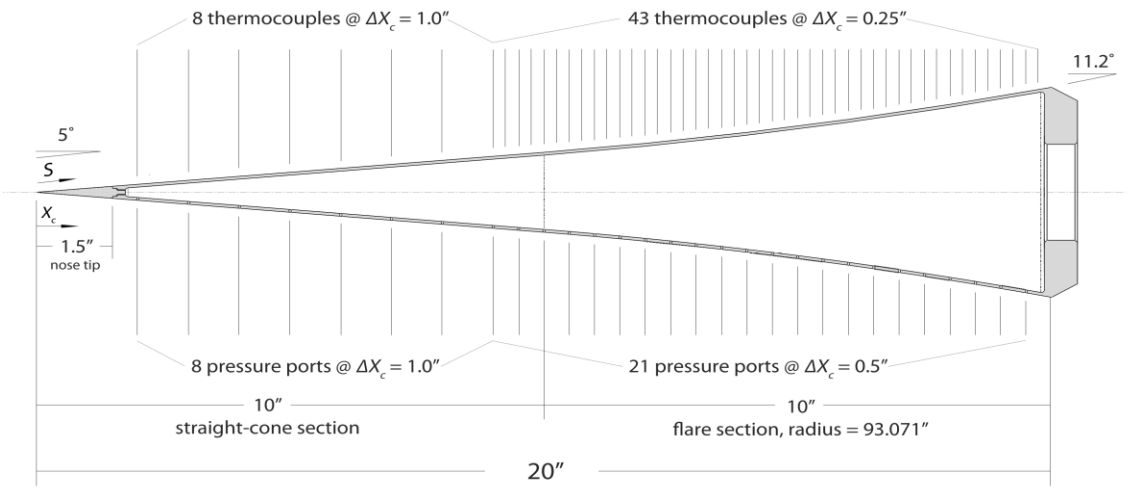

Fig. 3. Schematic of TAMU 93-10 Flare Cone.

B. Nonlinear Breakdown Simulation Setup

To simulate the non-linear breakdown during transition, the growths of spanwise wave modes play a crucial important role. Therefore, it is essential to conduct a 3D simulation. In the 3D non-linear simulation, only small degrees of arc in the circumferential direction of the cone are computed with periodic conditions enforced.

For the nonlinear unsteady simulation, a sponge layer needs to be added to the outflow to avoid spurious reflection and blowing up. In the sponge layer, an additional term is used to force the solution toward target values as shown in eq. (3). U is the place holder for any conservative variable. $A(\xi)$ is a weight function smoothly increases from 0 to 1. The steady flow values are used as the reference values in the equation, so that the flow will be forced back to laminar state.

$$\left(\frac{dU}{dt}\right)_{adj} = \frac{dU}{dt} - \sigma A(\xi)\left[U - U_{ref}\right] \tag{3}$$

$$A(\xi) = \frac{1}{t_{ref}} e^{-\xi^4/10}(1-\xi^{50})^4 \tag{4}$$

$$t_{ref} = \frac{u_\infty}{L_{buf}} \tag{5}$$

$$\xi = \frac{x_L - x}{L_{buf}} \quad (1 \geq \xi \geq 0) \tag{6}$$

C. Freestream Pulse Modeling

For the numerical study in this paper, we want to exam the linear receptivity response of freestream waves for a wide range of frequencies. In order to do so, we introduce a Gaussian pulse into the freestream that contains a continue frequency spectrum. Depending on the type of disturbance, The Gaussian pulse can be applied as acoustic waves, entropy waves, and vorticity waves. The formula of the pulse is the following:

$$q(x,t) = |q'| \exp\left(-\frac{\left(X_0 + x - c_\infty t\right)^2}{\sigma^2} \right), \quad \text{where } q = \langle \rho, u, v, w, p \rangle \tag{7}$$

In eq.(3), σ is the parameter dictates the band width of the Gaussian pulse. u is the pulse transport velocity which varies to the type of disturbance. For the case of fast acoustic pulse, u equals to $(u_\infty + a)$. Fig. 4 shows the pulse as function of time for $\sigma = 0.0012$ and its frequency spectrum assuming unity wave amplitude. This is the same pulse model we used on our TAMU Mach 6 case freestream receptivity simulation.

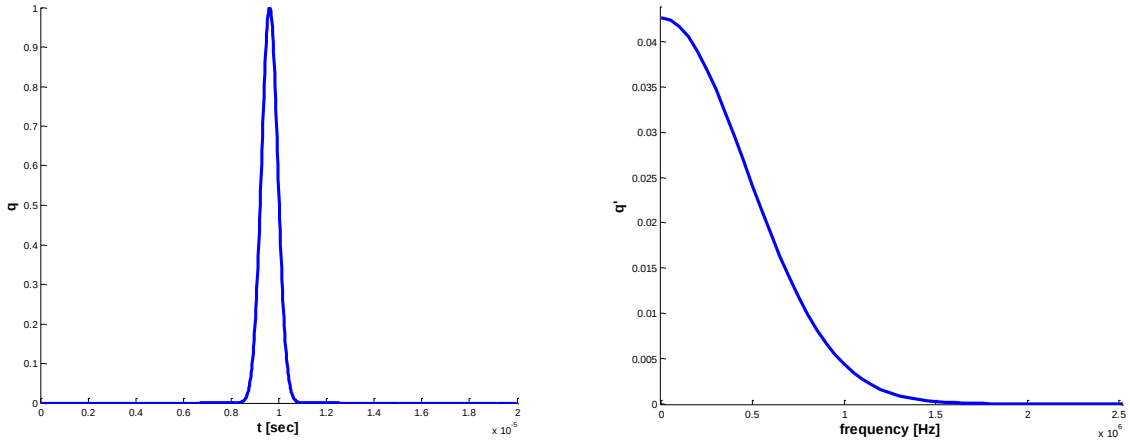

Fig. 4. Gaussian pulse function used for freestream fast acoustic wave and its frequency spectrum.

IV. Mean Flow and LST Calculations

A. Mean Flow Calculations

The mean flows are computed on two different cone models with the same freestream conditions. For the cone with nose radius of 0.125 inch, the first half is straight from the nose up to x=0.254 m and flared for the second half. This design is adapted purposely to shorten the transition process. A clear compression effect in the flared section is observed from the pressure contour in Fig. 5. The second cone model is a straight cone with 0.1 mm nose radius and 5 degrees half angle. As shown in Fig. 6, the straight cone has constantly thickening shock layer; and the surface pressure keeps decreasing along the downstream direction. In addition, because of the nose bluntness difference, the flare cone with blunter nose shows sign of entropy swallowing near the nose region in the Mach number contour.

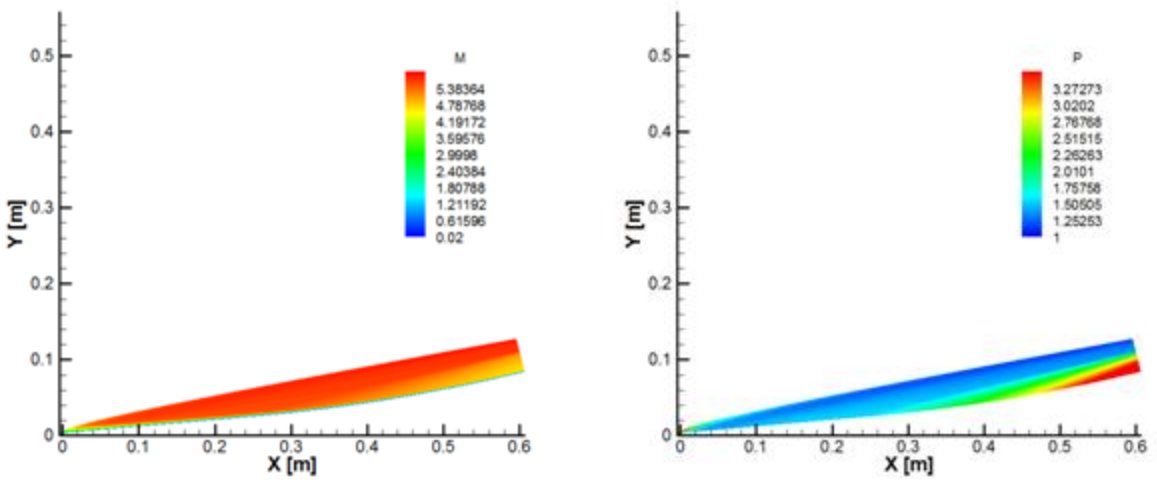

Fig. 5. Mach number contour and pressure contour for flare cone with 0.125 inch nose bluntness.

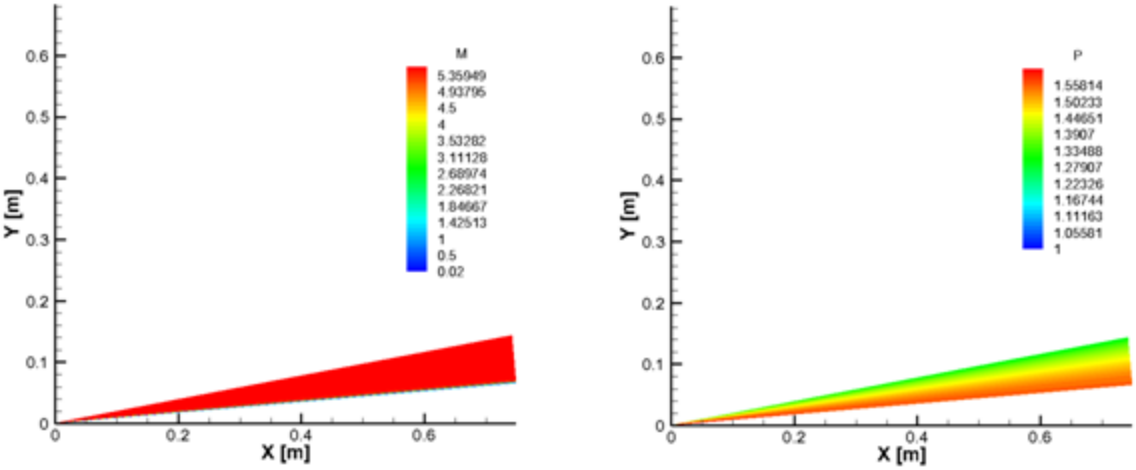

Fig. 6. Mach number contour and pressure contour for straight cone with 0.1 mm nose bluntness.

B. Linear Stability Analysis

The LST calculation is performed using the steady meanflow as the base flow solution. The *N* factor is calculated for the instability frequency. As shown in Fig. 7, due to the nose bluntness effect, the second mode instability appears only on the compression portion of the flare cone, while the instability appears much earlier for the "shape" straight cone. For the flare cone, the higher frequency wave becomes unstable at location further downstream. This is due to the compression effect causing reduction of boundary layer thickness at further downstream location. Based on the LST calculation, the sharper straight cone has higher N factor than the blunt flare cone.

To validate the LST calculation, the later linear receptivity result is used to compare with the LST. Fig. 8 shows the DNS and LST comparison of both growth rate and streamwise wave number of the disturbance wave at 144 kHz. Good agreement is obtained in the wave speed comparison between DNS and LST. However, the growth rate

comparison is a bit difficult because the instability wave is modulated with the stronger freestream forcing wave penetrating the shock. As the instability wave becomes more and more dominated further downstream, the DNS growth rate tends to converge with the LST calculation.

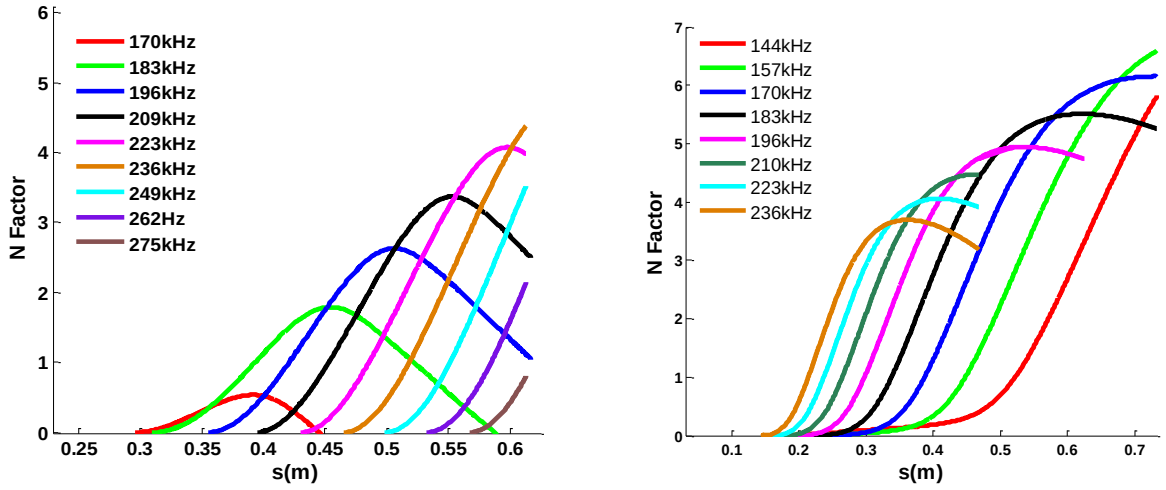

Fig. 7. *N* Factor for Selected Frequencies: (L) 0.125 inch flare cone, (R) 0.1 mm straight cone

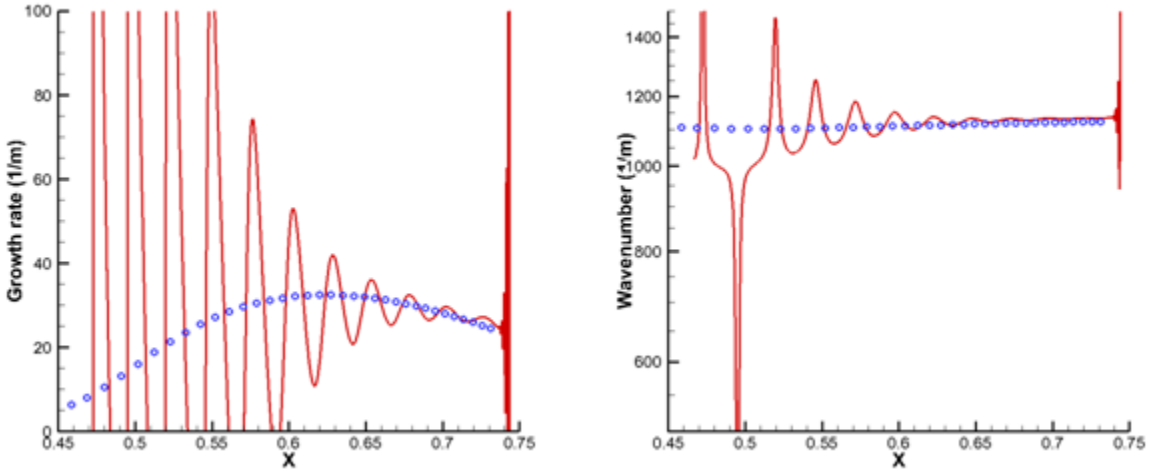

Fig. 8. Comparisons of DNS "—" and LST "o" results at 144 kHz for the 0.1mm nose bluntness case.

V. Freestream Receptivity

For the linear receptivity simulation, the freestream fast acoustic wave is used. The peak value of acoustic pulse is set to 0.05% of the freestream pressure. It is modeled as a planner wave in the upstream of the shock.

A. Nose Region Receptivity

As the second step of current numerical study, the linear receptivity simulation that captures the mechanism of freestream disturbance entering the bow shock and interacting with boundary layer is conducted. We only consider using one type of disturbance at a time to make the analysis easier. In this case, only the fast acoustic freestream

wave is imposed. Fig. 9 shows the snapshots of pressure contour of the receptivity simulation at the nose region of the 0.125 inch nose radius at different instances. At the nose region, the freestream acoustic pulse passed the bow shock and hit the cone surface then bounces off. As the wave reflected back from shock and hit the cone surface later at further downstream, the wave amplitude drops quickly and significantly. During this process, no boundary layer waves are excited yet.

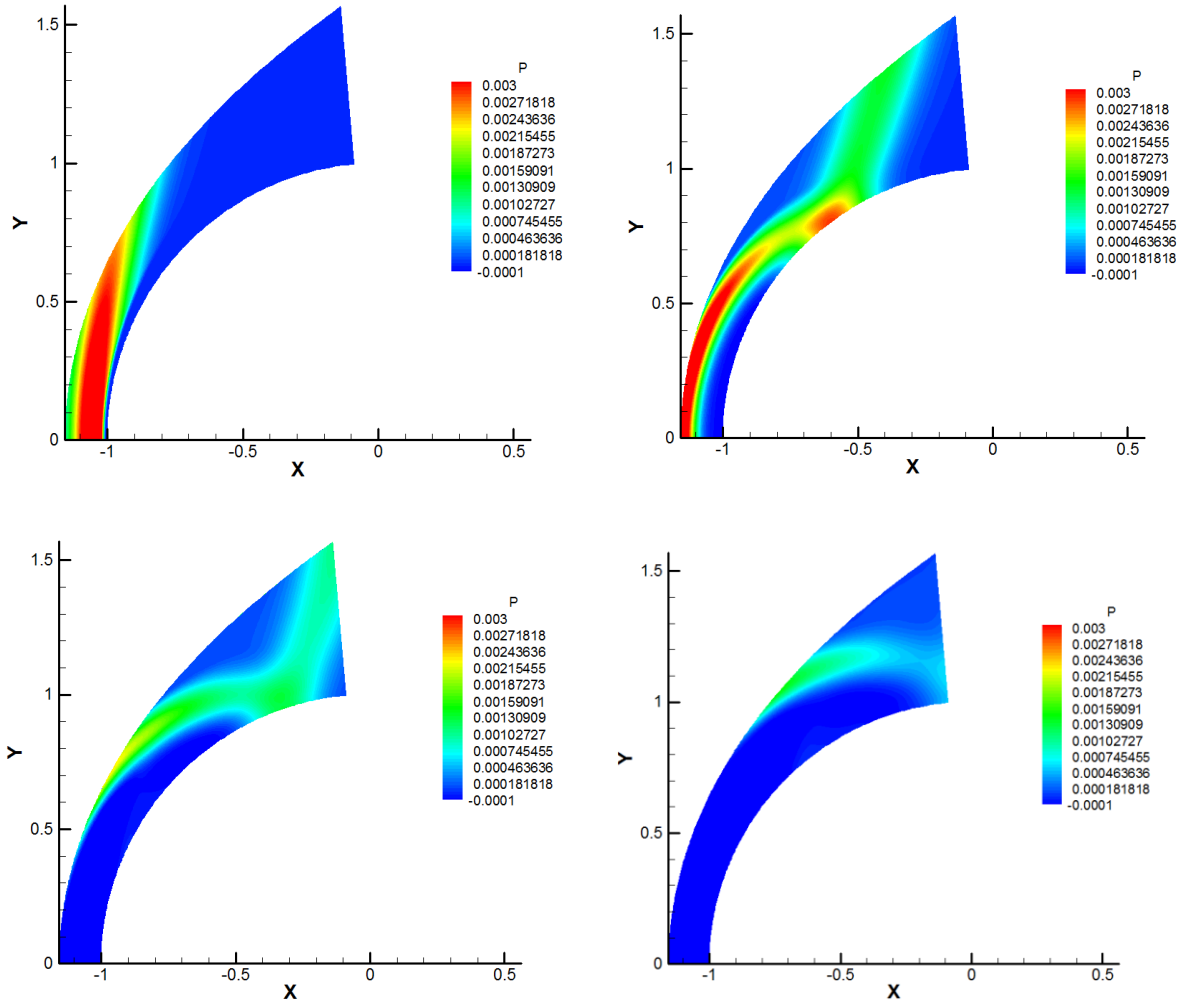

Fig. 9. Snapshots of pressure disturbance contour at the nose region (0.125 inch case).

Fig. 10 shows the pressure disturbance spectrum at the nose tip of the nose normalized the freestream wave spectrum. Two different responses are observed for the cones with different nose radius. For the 0.125 inch case, there are two peaks in the frequency spectrum, while the sharp cone shows no peak in the range of frequency showed. This intriguing result is believed to cause by the different bow shock stand-off distances. As shown in Fig. 11, the shock stand-off distance of the 0.125 inch nose radius case is about 0.5 mm, but it is only about 0.02 mm for the 0.1 mm nose radius cone case. Therefore, for the blunter nose, there is a resonance effect in the frequency range of interest. For the sharp cone, the resonance only occurs at very high frequency that it is totally out of the range we imposed in the freestream wave.

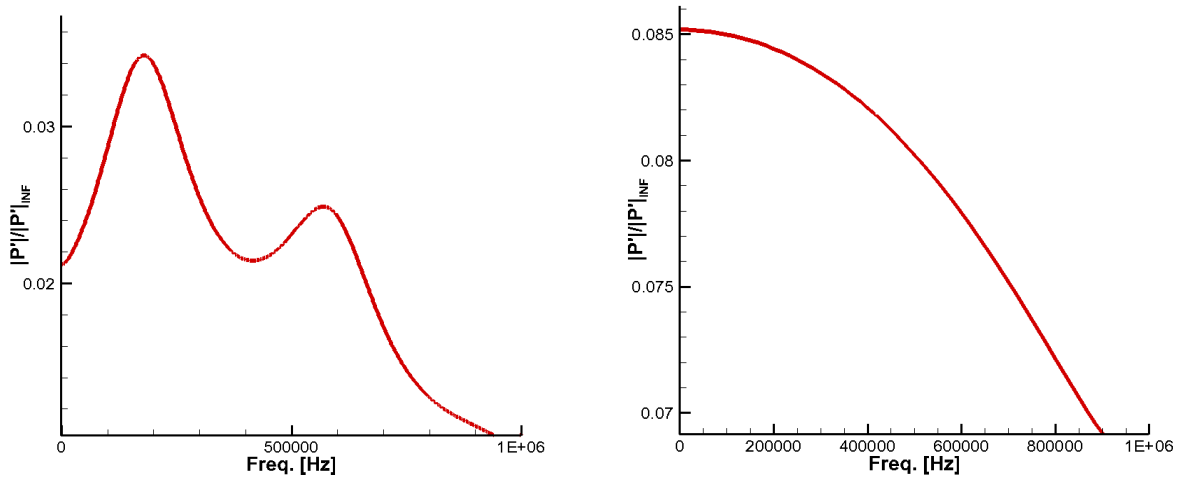

Fig. 10. Pressure disturbance spectrum normalized by the freestream: (L) 0.125 inch nose, (R) 0.1 mm nose.

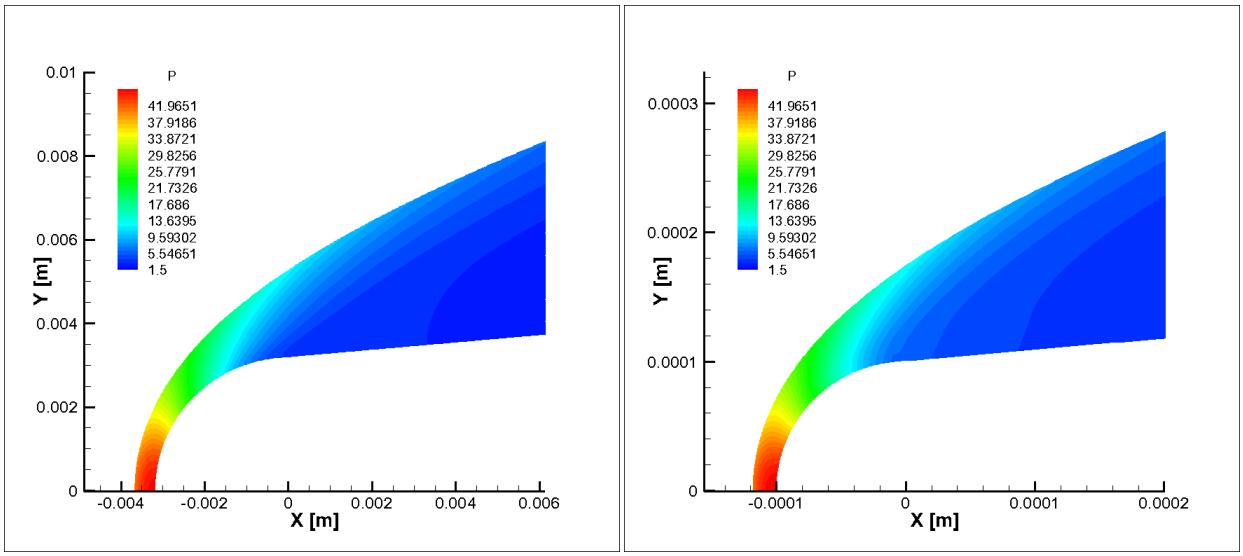

Fig. 11. Close-up pressure contours of nose regions: 0.125 inch nose (L), 0.1mm nose (R).

B. Linear Receptivity Simulation

As the wave keeps propagating down into the straight cone portion, the boundary layer modes start to emerge (Fig. 12). The amplitude of boundary layer waves sustains in the same order of magnitude as it moves further downstream. When the disturbances reach the unstable region as predicted by LST calculation, they quickly amplify. Fig. 13 shows the development of second mode instabilities in the more downstream locations along the cone surface.

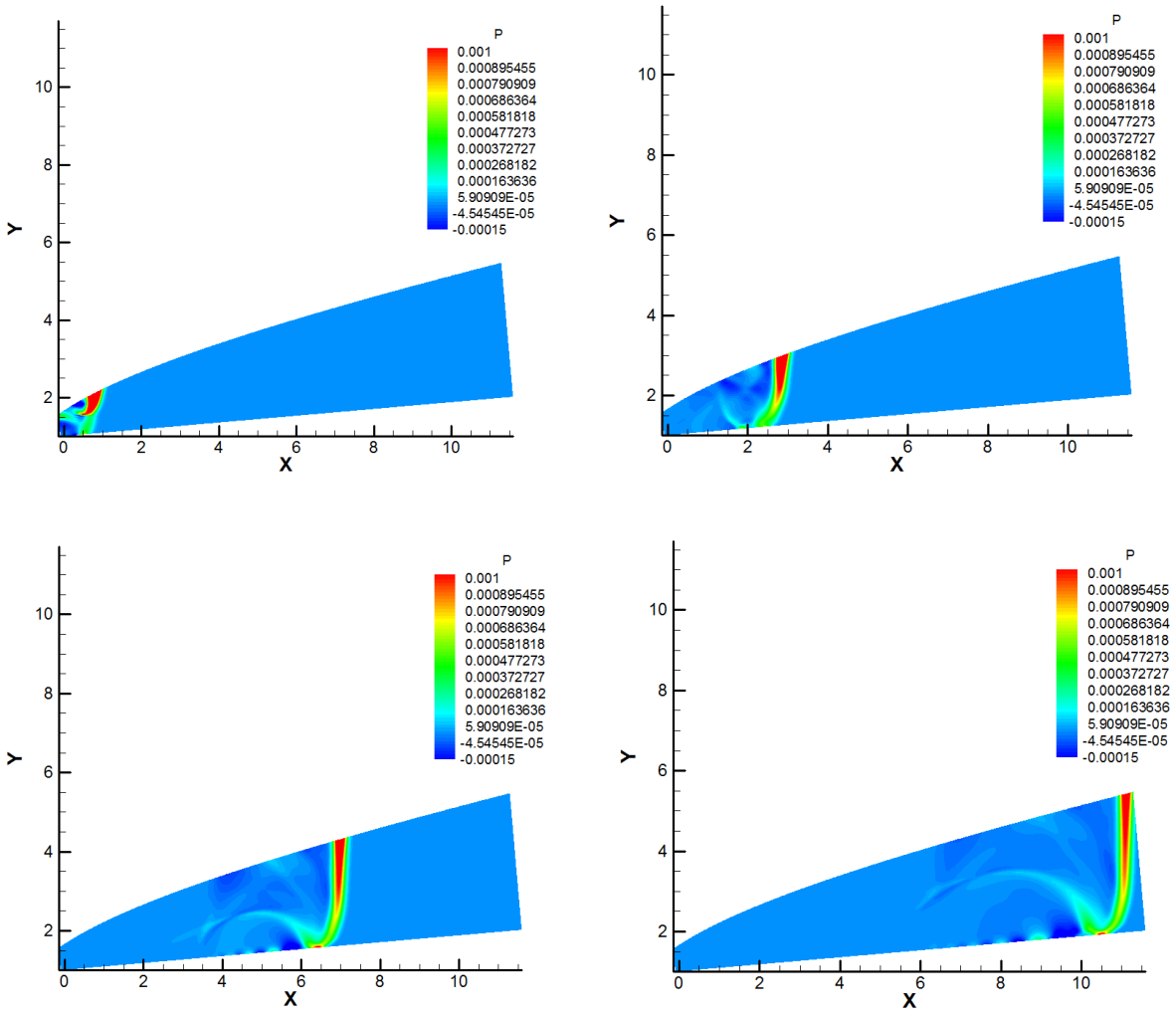

Fig. 12. Snap shot of pressure disturbance contour in the frustum of flare cone case.

From frequency spectrum, we can better track the evolution of wave disturbance as they propagate downstream. The disturbance wave amplitudes decay quickly in the nose region after passing through the bow shock. At the region after the nose, the wave spectrum kept oscillating while remained at comparable level. In the surface locations between x=0.115 m and x=0.252 m, there is a weak growing first mode region at frequency below 200 kHz. The unstable frequency quickly shifts toward the lower end as it moves downstream. The growth of first mode is very in-significant. At further downstream location, as predicted by LST calculation, the second mode instability emerged. As shown in Fig. 14, starting from location X=0.185 m, a spike is observed around 300 kHz. The second mode instability grows exponentially as it propagates in the downstream direction. Fig. 15 shows how the phase angles look across different frequency before and after the instability wave becomes dominated. At the early region along the cone surface, an organized repeating pattern is observed across all frequencies indicated that the freestream forcing wave is the most dominated wave inside boundary layer at that location. However, in the figure on the right, there is clearly a narrower pattern in the spectrum that distinguishes itself from other frequencies. This pattern falls into the second mode instability range.

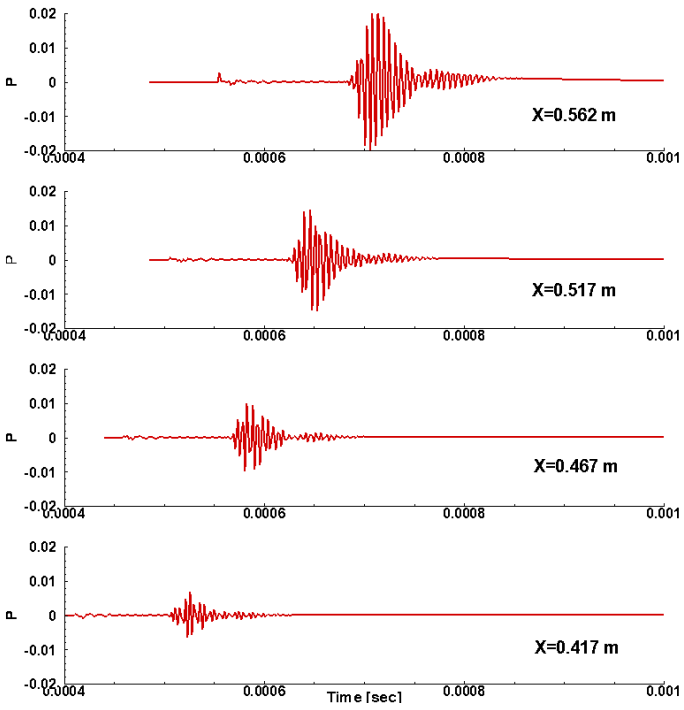

Fig. 13. Pressure disturbances time trace at different surface stations.

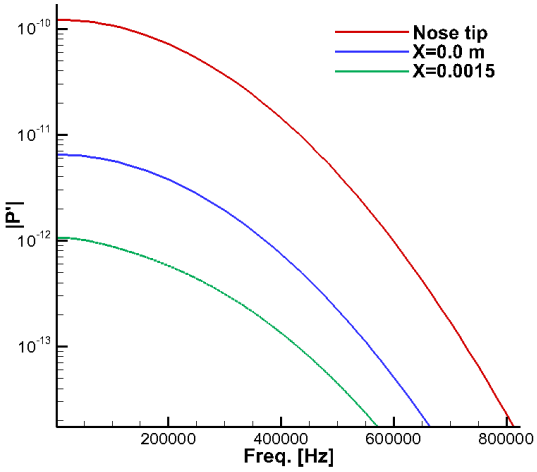

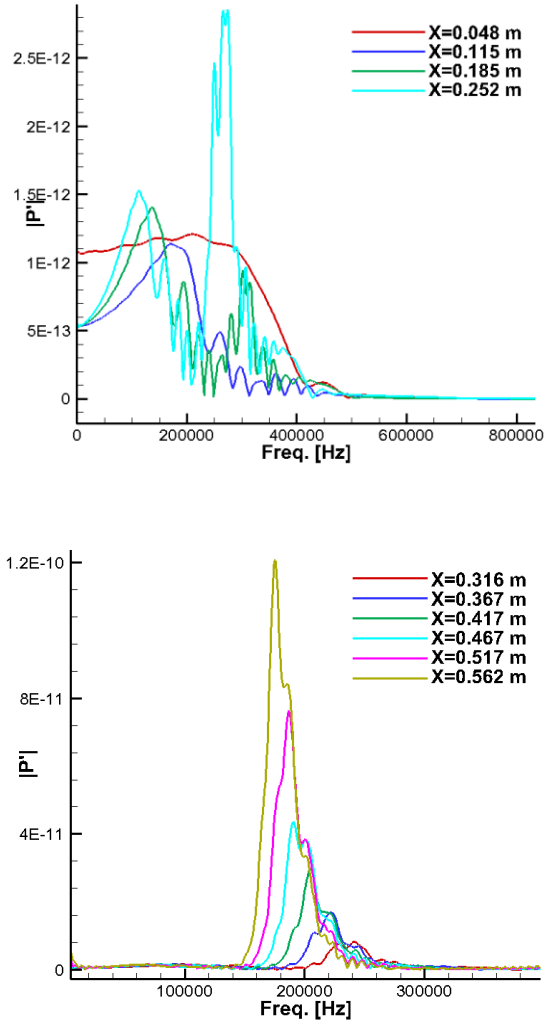

Fig. 14. Pressure Disturbances spectrum at different stations along the surface.

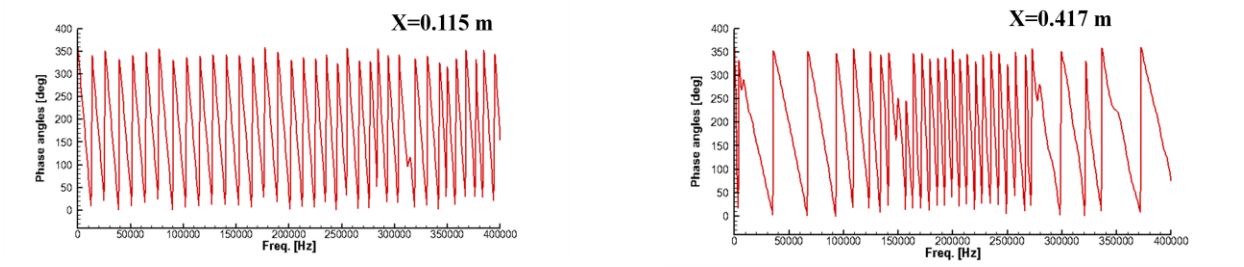

Fig. 15. Phase angles spectra on cone surface before (L) and after (R) the unsteady mode becomes dominant.

The freestream receptivity simulation is carried out to x=0.57 m, where the most amplified wave has an N factor about 6 according to the LST calculation. Fig. 16 shows the growths of disturbance waves in the second mode frequency range. The DNS result is consistent with the LST calculation.

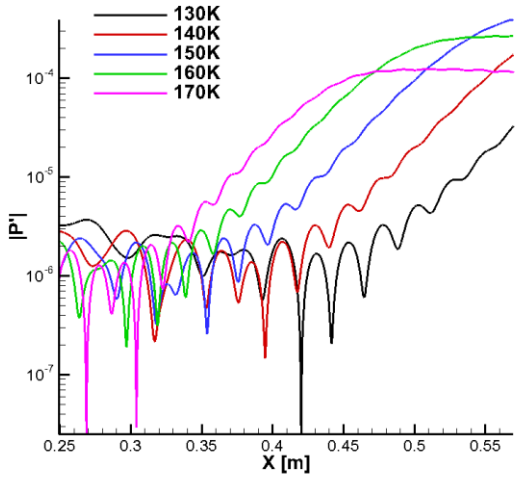

Fig. 16. Pressure disturbance along the surface at selected frequencies.

VI. Nonlinear Breakdown Simulation

A. Reconstruction of Inlet Disturbance Profile

The inlet disturbance profile is reconstructed using the receptivity results from the linear receptivity simulation. The original imposed profile is a Gaussian-shaped function, but the freestream wave spectrum from experiment is better fitted with an exponential function. As our first study case, we assume a simple exponential function as the freestream wave spectrum. In the future, the more reliable experimental data can be applied. Furthermore, the limitation on computational grids makes it difficult to resolve high frequency waves in current simulation. Therefore, all the higher frequency waves are truncated. Fig. 19 shows the inlet pressure disturbance time trace before and after the profile reconstruction.

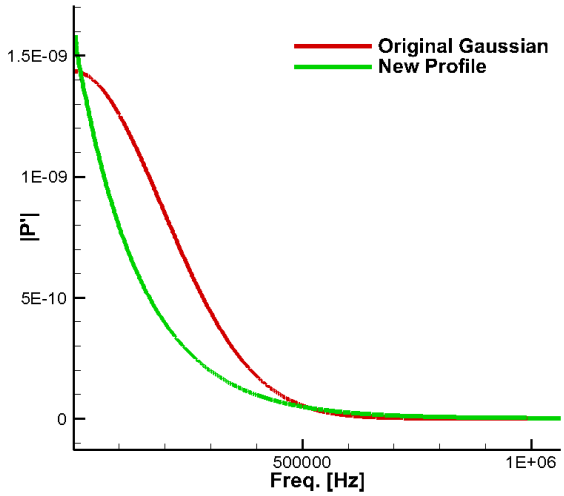

Fig. 17. Original Gaussian spectrum vs. exponential function spectrum.

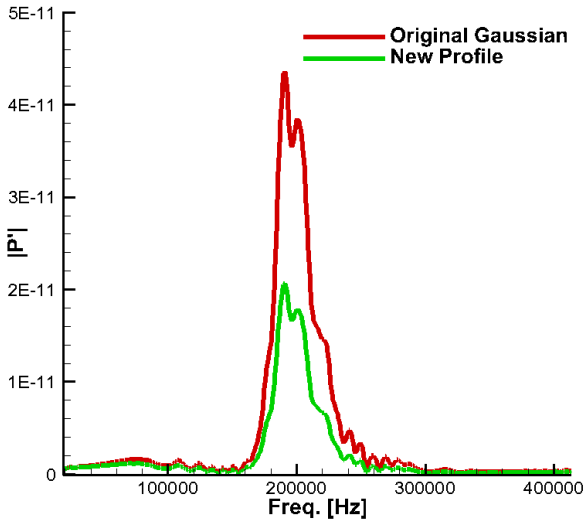

Fig. 18. Inlet pressure disturbance spectrum before and after reconstruction.

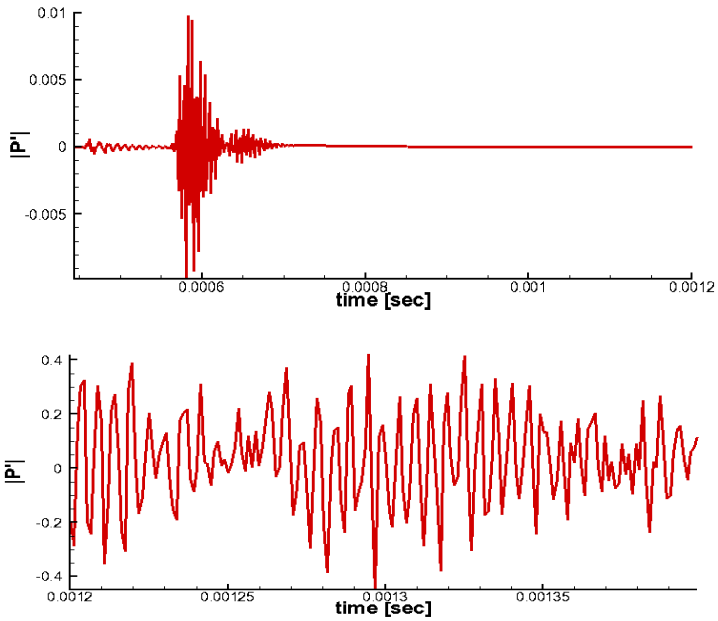

Fig. 19. Inlet pressure time trace before (upper) and after (lower) reconstruction.

B. Nonlinear Breakdown Simulation

The nonlinear simulation is carried from x=0.47 m to x=0.85 m using 3840 grid points in streamwise direction, 240 points in wall normal direction. 6 degrees arc in spanwise direction of the cone is resolved with 64 equally spaced grid points. The inlet is forced with pressure disturbance at 5% root-mean-square amplitude of its freestream pressure value. Fig. 20 shows the contour of pressure disturbance along the surface. In the early region of computational domain, a clear two dimensional second mode growth can be observed. The second mode growth reaches saturation in the middle of computational domain. Starting from location at x=0.78 m, some spanwise direction variation surfaces. This spanwise feature quickly amplifies and leads to breakdown. Fig. 21 further

demonstrates the breakdown by showing that the streamwise vorticity increases substantially when the spanwise fluctuation appears.

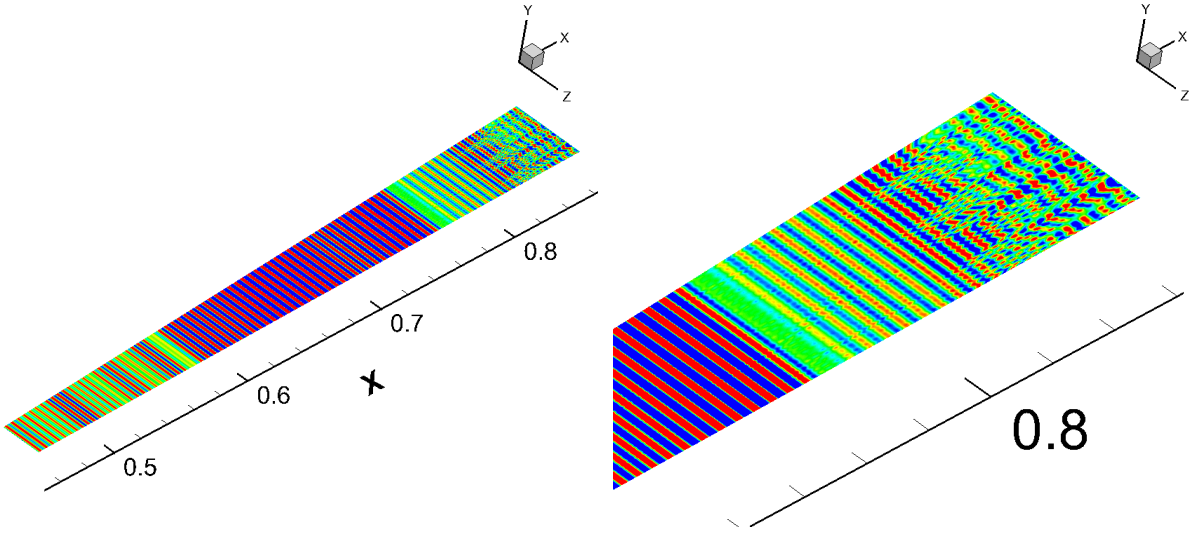

Fig. 20. Surface pressure disturbance contour.

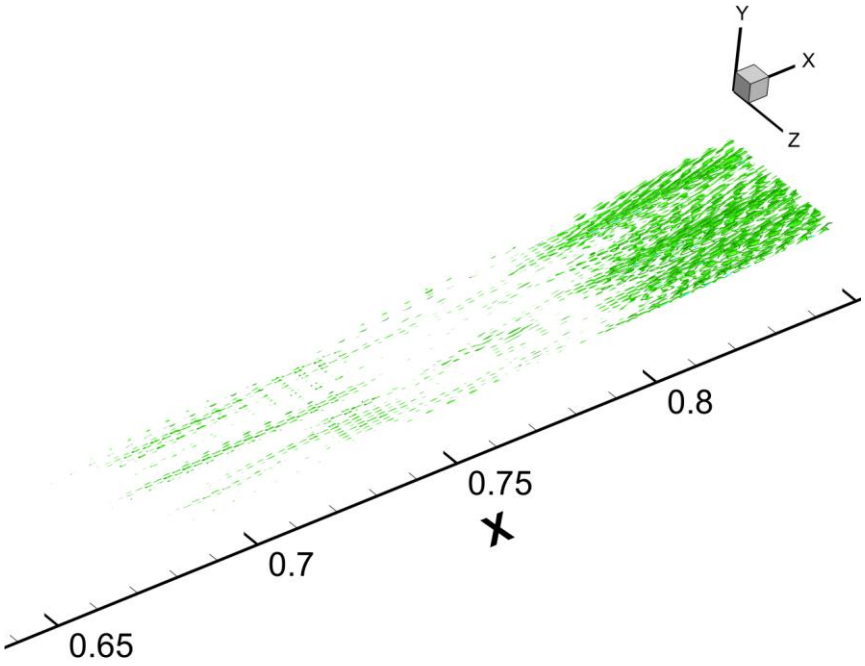

Fig. 21. Iso-surface contour of streamwise vorticity.

Fig. 22 shows the growths of primary 2D modes and most amplified 3D modes at the selected frequencies along the cone surface. At the inlet of computational domain, the spanwise modes start at the amplitude at least 3 order of magnitude lower than the primary 2D modes. Their exponential growths begin when the primary 2D modes reach saturation level. The frequency range of growing 3D modes is the same as the primary 2D modes which is the indication of fundamental breakdown mechanism.

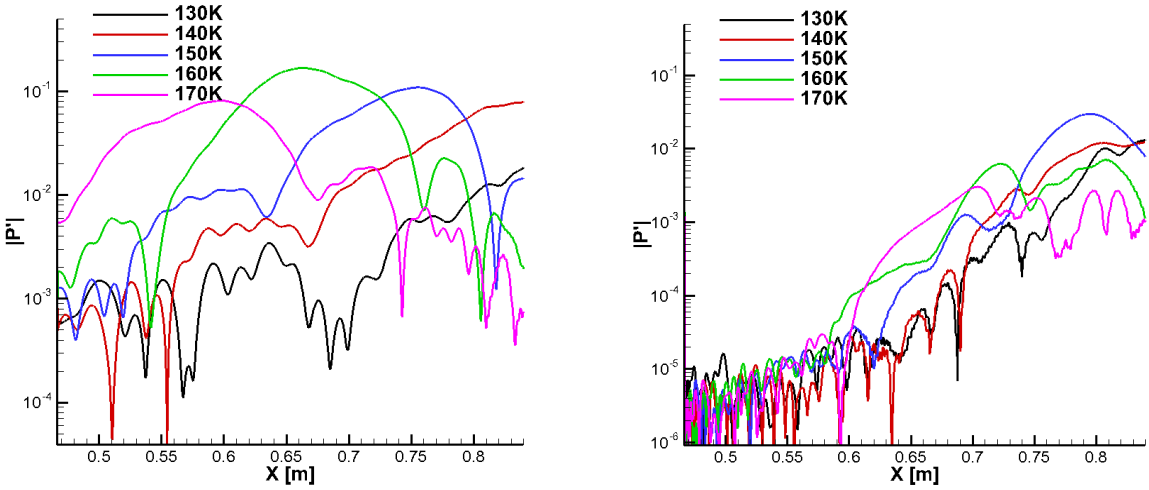

Fig. 22. Pressure disturbance amplitudes at selected frequencies: (L) *K*=0 /m, (R) *K*=1860 /m.

To better understand the breakdown mechanism, Fourier analysis is applied to decompose the disturbance waves in both frequency domain and spanwise wave number domain. Fig. 23 shows the pressure disturbance amplitude of each wave modes in spanwise wave number - frequency plane at the inlet and near the exit of nonlinear breakdown simulation computational domain. At x=0.47 m, the Fourier analysis shows that the instability is primarily two dimension. Near the exit (at x=0.84 m), the 3D wave modes with higher spanwise wave numbers are highly amplified. There is clearly fundamental resonance where the most amplified wave mode at higher have the same frequency as the second mode instability wave. Also, at some lower wave numbers between K=200 and K=600. There are three peaks in wave number that are highly amplified. That could be the oblique break down mechanism. However, further investigation is needed to verify it. From Fig. 24, there is a small peak near frequency around 100 kHz in the most amplified spanwise wave numbers. This frequency is much lower than the second mode frequency. This could be an indication of sub-harmonic resonance mechanism.

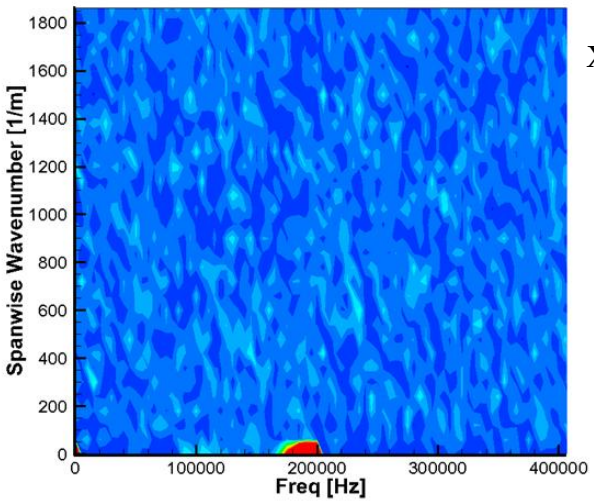

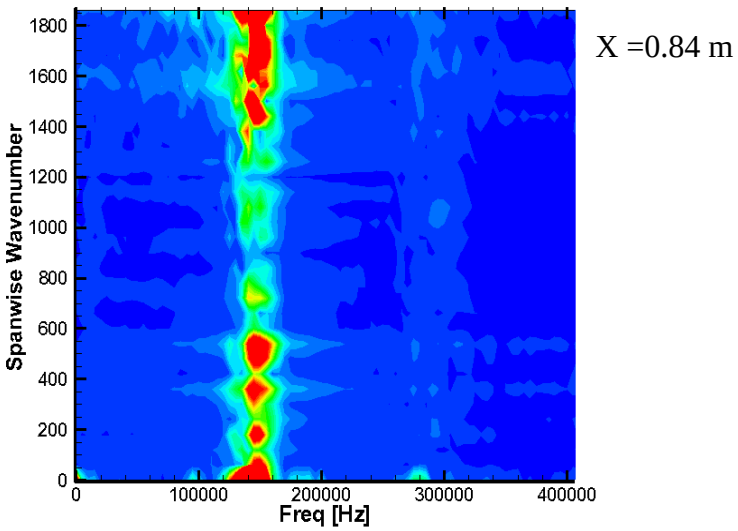

Fig. 23. Disturbance amplitude in spanwise wave number – frequency plane at different surface locations.

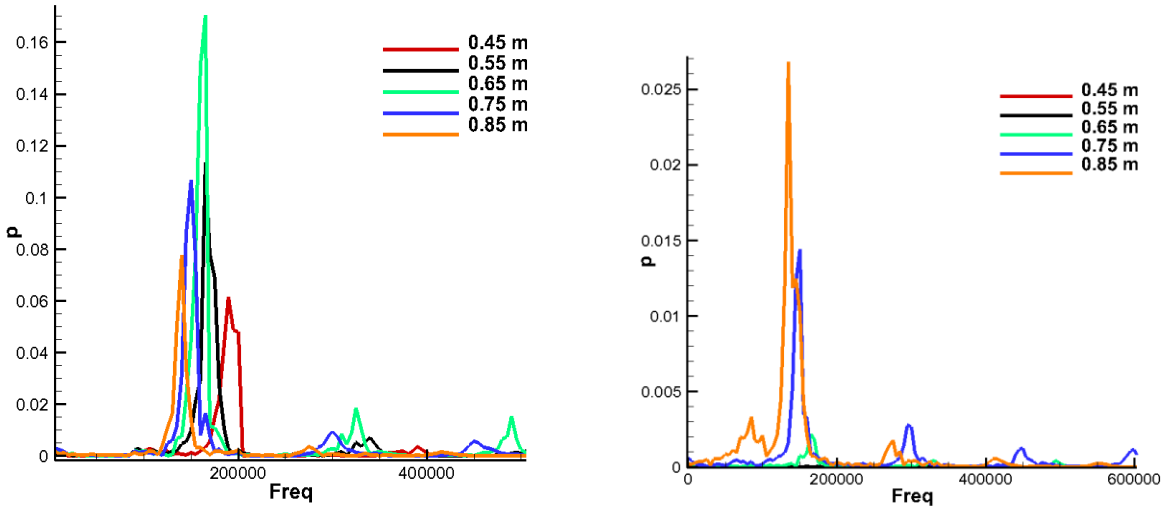

Fig. 24. Pressure disturbance spectra of 2D wave modes (L) and most amplified oblique wave modes (R).

VII. Conclusion and Remarks

In this paper, we demonstrated the feasibility of our approach to conduct hypersonic boundary layer transition simulation induced by freestream waves. Also, some early works on our study case are presented. One study case of straight cone with nose bluntness of 0.1 mm over Mach 6 flow has been completed using the proposed three-step approach. From the current study, we observe the fundamental breakdown as the key player in the hypersonic boundary layer transition process. However, the presences of sub-harmonic resonance and oblique breakdown are still under investigation. We are currently in progress of running more nonlinear breakdown simulation cases to better understand how the initial amplitudes of primary wave and white noise level affect the breakdown as well as how different breakdown mechanisms act together leading to hypersonic boundary layer transition.

Acknowledgments

This work was sponsored by AFOSR/NASA *National Center of Hypersonic Research in Laminar-Turbulent Transition*, and under grant No.FA9550-07-1-0414, monitored by Dr. John Schmisseur. The authors also thank XSEDE and AFOSR for providing computational time from their high performance supercomputer systems. The views and conclusions contained herein are those of authors and should not be interpreted as necessarily representing the official policies or endorsement either expressed or implied, of the Air Force Office and Scientific research or U.S Government.

References

1. Kimmel, R.L., *Aspects of Hypersonic Boundary-Layer Transition Control.* 41st Aerospace Sciences Meeting and Exhibit, 2003. **AIAA paper 2003-0772**: p. 1-21.
2. Saric, W.S., Reed, H. L., and Kerschen, E. J., *Boundary-Layer Receptivity to Freestream Disturbances.* Annual Review of Fluid Mechanics, 2002. **34**: p. 291-319.
3. Pruett, C.D., Zang, T. A., Chang, C. L., and Carpenter, M. H., *Spatial Direct Numerical Simulation of High-Speed Boundary-Layer Flows, Part I: Algorithmic Considerations and Validation.* Theoretical and Computational Fluid Dynamics, 1995. **7**: p. 49-76.
4. Pruett, C.D.a.C., C. L., *Spatial direct numerical simulation of high-speed boundary-layer flows Part II: Transition on a cone in Mach 8 flow* Theoretical and Computational Fluid Dynamics, 1995. **7**: p. 397-424.
5. Erlebacher, G., Hussaini, M. Y., *Numerical Experiments in Supersonic Boundary-Layer Stability.* Physics of Fluids A, 1990. **2**(1): p. 94-104.
6. Erlebacher, G.a.H., M. Y., *Stability and Transition in Supersonic Boundary Layers.* AIAA Paper 1987-1416, 1987: p. 1-12.
7. Thumm, A., Wolz, W., and Fasel, H. *Numerical simulation of spatially growing three-dimensional disturbance waves in compressible boundary layers*. in *Laminar-Turbulent Transition. IUTAM Symposium*. 1990. Toulouse, France, 1989 Springer-Verlag, Berlin.
8. Fasel, H., Thumm, A., and Bestek, H. *Direct numerical simulation of transition in supersonic boundary layers: oblique breakdown*. in *Fluids Engineering Conference, Transitional and Turbulent Compressible Flows*. 1993. Washington, DC, June 20–24, 1993: ASME, New York.
9. Chang, C.-L.a.M., M. R., *Oblique-mode breakdown and secondary instability in supersonic boundary layers.* Journal of Fluid Mechanics, 1994. **273**: p. 323-360.
10. Sandham, N.D., Adams, N. A., Kleiser, L., *Direct simulation of breakdown to turbulence following oblique instability waves in a supersonic boundary layer.* Applied Scientific Research, 1995. **54**: p. 223-234.
11. Mayer, C.S.J., von Terzi, D. A., and Fasel, H. F., *DNS of Complete Transition to Turbulence Via Oblique Breakdown at Mach 3.* AIAA paper 2008-4398, 2008: p. 1-21.
12. Laible, A., Mayer, C., and Fasel, H., *Numerical Investigation of Supersonic Transition for a Circular Cone at Mach 3.5*. AIAA paper 2008-4397 2008: p. 1-24.
13. Husmeier, F., Fasel, H. F., *Numerical Investigations of Hypersonic Boundary Layer Transition for Circular Cones.* AIAA paper 2007-3843, 2007: p. 1-17.
14. Stetson, K.F., Thompson, E. R., Donaldson, J. C., and Siler, L. G., *Laminar Boundary Layer Stability Experiments on a Cone at Mach 8, Part 1: Sharp Cone.* 1983. **AIAA Paper 83-1761**.
15. Stetson, K.F., Thompson, E. R., Donaldson, J. C., and Siler, L. G., *Laminar Boundary Layer Stability Experiments on a Cone at Mach 8, Part 2: Blunt Cone.* 1984. **AIAA paper 84-0006**.
16. Pruett, C.D.a.C., C. L., *Direct Numerical Simulation of Hypersonic Boundary-Layer Flow on a Flared Cone* Theoretical and Computational Fluid Dynamics, 1998. **11**: p. 49-67.
17. Zhong, X., *High-Order Finite-Difference Schemes for Numerical Simulation of Hypersonic Boundary-Layer Transition.* Journal of Computational Physics, 1998. **144**: p. 662-709.